Impact of Dynamics and Atmospheric State on Cloud Vertical Overlap

CATHERINE M. NAUD

Department of Applied Physics and Applied Mathematics, Columbia University, and NASA Goddard Institute for Space Studies, New York, New York

ANTHONY DEL GENIO

NASA Goddard Institute for Space Studies, New York, New York

GERALD G. MACE AND SALLY BENSON

Department of Meteorology, University of Utah, Salt Lake City, Utah

EUGENE E. CLOTHIAUX

Department of Meteorology, The Pennsylvania State University, University Park, Pennsylvania

PAVLOS KOLLIAS

Department of Atmospheric and Oceanic Sciences, McGill University, Montreal, Quebec, Canada

(Manuscript received 20 December 2006, in final form 22 August 2007)

ABSTRACT

The observation and representation in general circulation models (GCMs) of cloud vertical overlap are the objects of active research due to their impacts on the earth's radiative budget. Previous studies have found that vertically contiguous cloudy layers show a maximum overlap between layers up to several kilometers apart but tend toward a random overlap as separations increase. The decorrelation length scale that characterizes the progressive transition from maximum to random overlap changes from one location and season to another and thus may be influenced by large-scale vertical motion, wind shear, or convection. Observations from the U.S. Department of Energy Atmospheric Radiation Measurement program ground-based radars and lidars in midlatitude and tropical locations in combination with reanalysis meteorological fields are used to evaluate how dynamics and atmospheric state influence cloud overlap. For midlatitude winter months, strong synoptic-scale upward motion maintains conditions closer to maximum overlap at large separations. In the tropics, overlap becomes closer to maximum as convective stability decreases. In midlatitude subsidence and tropical convectively stable situations, where a smooth transition from maximum to random overlap is found on average, large wind shears sometimes favor minimum overlap. Precipitation periods are discarded from the analysis but, when included, maximum overlap occurs more often at large separations. The results suggest that a straightforward modification of the existing GCM mixed maximum–random overlap parameterization approach that accounts for environmental conditions can capture much of the important variability and is more realistic than approaches that are only based on an exponential decay transition from maximum to random overlap.

1. Introduction

The vertical distribution of cloudy layers has important implications for the radiative budget and heating rate profiles in general circulation models (GCMs) (Chen et al. 2000; Morcrette and Jakob 2000). Since the appearance of the study by Geleyn and Hollingsworth (1979), a common assumption has been that cloud layers separated by clear (i.e., cloud free) air exhibit a random overlap while vertically contiguous cloudy sublayers within a cloudy layer exhibit a maximum overlap. Using ground-based radar cloud profiles from Chilbolton

Corresponding author address: Catherine Naud, NASA GISS, 2880 Broadway, New York, NY 10025.
E-mail: cnaud@giss.nasa.gov

DOI: 10.1175/2007JCLI1828.1

(United Kingdom) during three winter months, Hogan and Illingworth (2000) found that cloudy sublayers within the same cloud layer only showed a maximum overlap when they were close to each other. As separations between cloudy sublayers within a cloud layer increase (e.g., greater than about 2 km), they observed that the overlap became random. Using the same technique as introduced by Hogan and Illingworth (2000), Mace and Benson-Troth (2002) analyzed radar vertical profiles at the Atmospheric Radiation Measurement (ARM; Ackerman and Stokes 2003) program sites of the North Slope of Alaska (NSA), the southern Great Plains (SGP), and the two tropical west Pacific (TWP) sites of Manus and Nauru. Their conclusions differed somewhat from those of Hogan and Illingworth (2000). At the NSA site, cloudy layers behaved in a rather similar manner as observed at Chilbolton, but at SGP and the two TWP sites, cloudy sublayers within the same cloud tended to exhibit maximum overlap for much larger separations than was found at NSA or Chilbolton. This hindered the generalization of the relationship between overlap type and layer separation. Mace and Benson-Troth (2002) also found seasonal variations at SGP: Cloudy sublayers within the same cloud exhibit a transition from maximum to random overlap for larger separations during summer than winter.

These findings suggest that factors such as dynamics could be connected to the way cloudy layers overlap. Indeed, Pincus et al. (2005) found from cloud-resolving model (CRM) simulations that stratiform and convective clouds have different overlap properties with some connections between shear and convective activity and overlap type. Their study was limited to deep convective events during one midlatitude summer month and relied on the accuracy of their two-dimensional simulations.

Overlap affects cloud areal fraction and thus cloud radiative forcing, and the observed seasonal and geographical variations suggest a dependence on environmental state that could result in a contribution to cloud feedback in a climate change. Here, we use ground-based radar and lidar observations in conjunction with information on the state of the atmosphere derived from meteorological reanalyses to investigate the impact of large-scale dynamics and atmospheric state on cloud overlap. Section 2 describes the various datasets used in this study, briefly presents the method, and discusses uncertainties associated with sampling limitations. Section 3 presents the overlap properties at SGP and TWP and discusses their relation to the dynamics and atmospheric state. Finally, section 4 presents a discussion and the conclusions, including implications for overlap parameterization.

2. Data

The datasets used for this study are described below and the expected accuracy of the overlap information retrieved from the radar cloud data is estimated.

a. Meteorological reanalysis datasets

To characterize the synoptic situation at SGP, we use 20-km resolution hourly three-dimensional meteorological fields from the Rapid Update Cycle (RUC-2) reanalysis (Benjamin et al. 1998) produced at the National Centers for Environmental Prediction (NCEP). This dataset is available from April 2002, and because the radar products at SGP were not available at the time of this study beyond September 2004, these dates dictated the 2-yr period chosen here. Temperature, geopotential height, and horizontal wind speed profiles, together with 500-mb vertical velocities, are extracted for the SGP site. Because this high-resolution dataset is not available for the TWP sites, there we use instead 2.5°-resolution NCEP–National Center for Atmospheric Research (NCAR) 6-hourly reanalysis profiles of the same quantities (Kalnay et al. 1996; Kistler et al. 2001).

b. Radar data

We analyze 2 yr of processed 35-GHz millimeter-wave cloud radar (MMCR) data (Moran et al. 1998) from September 2002 through August 2004 at the SGP ARM site (36.62°N, 97.5°W), from July 1999 through June 2001 at the TWP-Manus site (2.006°S, 147.425°E), and from January 1999 through December 2000 at the TWP-Nauru site (0.521°S, 166.916°E). The active remotely sensed cloud locations (ARSCLs; Clothiaux et al. 2000) product combines radar reflectivities and micropulse lidar returns to provide a 10-s- and 45-m-resolution cloud mask. This cloud mask classifies each pixel as clear, cloudy, a mixture of hydrometeors and clutter, or pure clutter. Clutter can be insects or airborne vegetation debris and is a severe problem in the SGP cloud radar data during the warm season.

At present there is no simple method to decipher clutter from hydrometeors in the radar returns, and this prevents accurate cloud detection from the ground to altitudes as high as 5 km. Consequently, we decided to ignore the summer months at SGP. The ARSCL files also contain a precipitation flag. At the SGP site, the precipitation flag indicates when a nearby microwave radiometer wet window sensor strip automatically de-

tects rain drops (indicating that the radiometer antenna most likely has water on it). This device does not give a quantitative rainfall rate and is not sensitive to virga, but is believed to be qualitatively more sensitive than tipping buckets to light precipitation that reaches the ground. At the TWP sites, the ARSCL precipitation flag contains information from an optical rain gauge. Using the condensation strip sensor flag at SGP and the optical rain gauge at TWP, if an hour of data has precipitation detected at the ground at some point in time, the entire hour is removed from our study.

c. Assessment of method accuracy

A complete description of the method used to derive overlap between noncontiguous pairs of cloudy layers, as well as cloudy sublayers within a cloud layer, using radar data can be found in Hogan and Illingworth (2000, hereafter referred to as HI00). The radar cloud mask time series are used to define 360-m vertical and 1-h horizontal cloudy layers. The overlap of two cloudy layers of fractions $0 < (C_1, C_2) < 1$ is characterized by using the overlap parameter α defined as follows:

$$C_{\text{true}} = \alpha C_{\max} + (1 - \alpha) C_{\text{rand}}, \tag{1}$$

where C_{true} is the actual cloud fraction of the two layers, $C_{\text{rand}} = C_1 + C_2 - C_1C_2$ and $C_{\max} = \max[C_1, C_2]$. When $\alpha = 1$, the two cloud layers exhibit a maximum overlap and when $\alpha = 0$, the overlap is random. When $\alpha < 0$, $C_{\text{true}} > C_{\text{rand}}$ and the overlap tends toward the minimum with a fraction $C_{\min} = \min[1, C_1 + C_2]$.

All available pairs of cloudy layers in the 2-yr radar dataset that occurred in periods when no precipitation was detected on the ground (precipitating particles can cause too many occurrences of maximum overlap; see the appendix) are then placed into either one of two subsets depending on whether or not the two layers are in vertically contiguous cloudy air. The corresponding α's are then averaged as a function of layer separation distance. To describe the relationship between the overlap parameter and the separation distance when the pairs are in vertically contiguous cloudy air, HI00 proposed an exponential fit:

$$\overline{\alpha} = e^{-\frac{\Delta z}{z_0}}, \tag{2}$$

where Z_0 is the decorrelation length scale that characterizes the progressive transition from maximum overlap at low separation to random overlap at large separation.

Since our objective is to differentiate random ($\alpha = 0$) from maximum ($\alpha = 1$) overlap, we investigated the impact of an error in α of 0.1 on the radiation fields. We collected broadband shortwave (SW) cloud forcing and cloud fraction measurements from the SGP site for the same time period from the ARM Shortwave Flux Analysis (Long et al. 1999; Long and Ackerman 2000). Using the time of day when the cosine of the solar

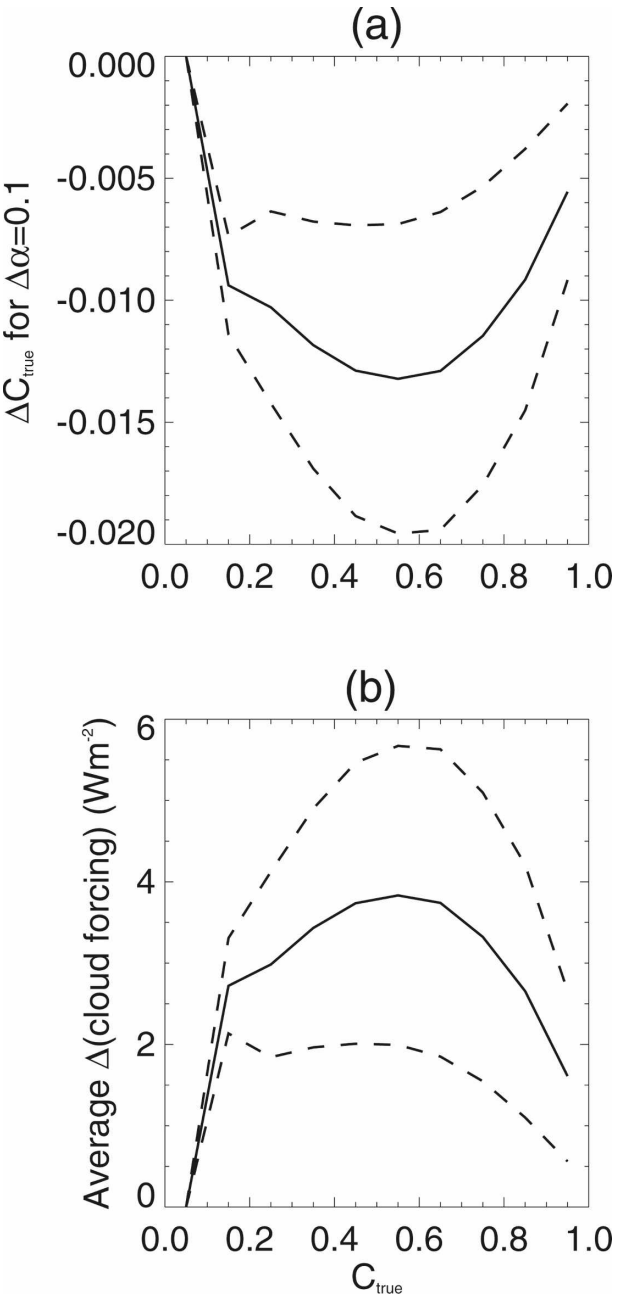

FIG. 1. (a) Change in C_{true} (or column total cloud fraction) induced by a change in the overlap parameter α of 0.1 as a function of total cloud fraction C_{true} averaged over all possible values of two cloud-layer cloud fractions ($0 < C_1 < 1$ and $0 < C_2 < 1$) and all possible values of their overlap parameter ($0 \leq \alpha \leq 1$) in 0.1 increments (solid). The dashed lines indicate ± 1 std dev. (b) Corresponding change in shortwave downward cloud forcing as a function of C_{true} (solid). The dashed lines indicate ± 1 std dev.

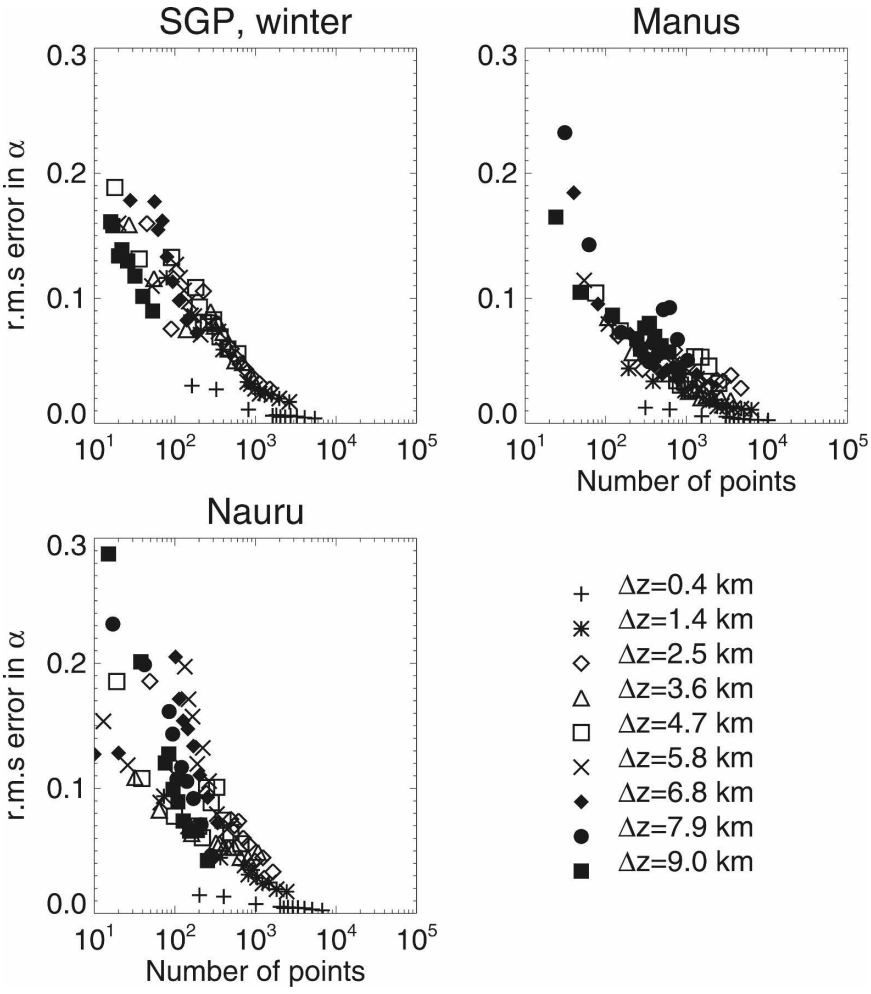

FIG. 2. The rms error in α as a function of the number of points for a variety of layer separations. Results are presented for 2 yr of data from each of the three sites: (top left) SGP-winter, (top right) Manus, (bottom left) Nauru, and (bottom right) key. Each symbol represents the standard error in mean α obtained from the total dataset and 100 possible subsets of a given number of points. The different symbols represent different layer separations.

zenith angle is maximum, a linear regression of the mean cloud forcing per 0.1 cloud fraction bin is performed. Assuming a column containing two cloud layers of varying cloud fractions (C_1 and C_2) and overlap ($0 \leq \alpha \leq 1$), we calculated for all possible triplets (C_1, C_2, α) the average change in C_{true} caused by a change in α of 0.1 as a function of C_{true} (Fig. 1a). For each possible C_{true}, we can then directly relate this average change in C_{true} to the change in cloud forcing (Fig. 1b). For cloud fractions C_{true} in the range 0.5–0.6, where the change in α induces the greatest change in C_{true}, the change in cloud forcing is 4 ± 2 W m^{-2} (about 10% of the mean cloud forcing), which is close to the expected uncertainty of the measurements (Long and Ackerman 2000) and can be considered as a value above which differences in cloud forcing start to be significant. Consequently, errors in α of magnitude 0.1 or less are considered acceptable.

Errors in α can occur due to the limited sampling. We examine how decreasing the number of points from our original datasets at SGP, Manus, and Nauru modifies the values of mean α at all separations. Starting with the full dataset we randomly and independently select 100 subsets with an equal number of points, calculate the difference in mean α between the full dataset and each subset, and then estimate the standard deviation of the difference in mean α. We repeat the same operation for different sizes of the subsets. Figure 2 shows, for each separation, the rms error in α as a function of the number of points per subset for the three locations. The rms error decreases with the number of points N as $1/\sqrt{N}$, independent of layer separation except at the smallest

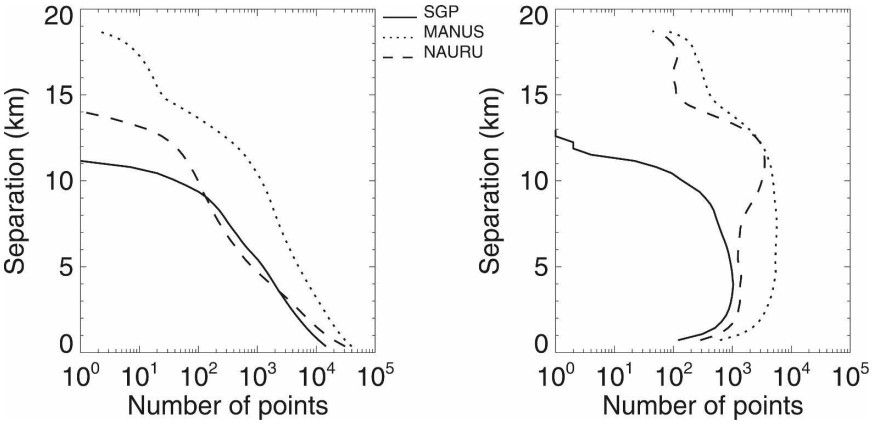

FIG. 3. Number of points used to calculate the average α as a function of layer separation for SGP (solid line), Manus (dotted line), and Nauru (dashed line) for (left) contiguous and (right) noncontiguous cloud layers.

separation for which α is close to 1 and the variability is limited. Figure 2 shows that a sample of a minimum of 250 points assures an error in α of no greater than 0.1 at any of the sites. Thus, we ignore all separations for which there are fewer than 250 points.

Errors introduced by the choice of radar cloud mask are analyzed in the appendix and are found to be within the 0.1 α requirement.

3. Dependence of overlap behavior on dynamic and thermodynamic state

The average behavior of α as a function of cloud-layer separation in vertically contiguous cloudy air is first described and its behavior for different dynamical situations and different atmospheric states is then discussed.

a. Average overlap behavior

Figure 3 shows for the three sites the number of points available per cloud-layer separation. The 250-point cutoff value indicates the maximum altitude sampled here for each location and each subset (layers in vertically contiguous or vertically noncontiguous cloudy air). Figure 4 shows the mean α as a function of layer separation at the three locations.

In accordance with HI00 and Mace and Benson-Troth (2002, hereafter referred to as MBT02), contiguous cloud layers at the three locations display maximum overlap ($\alpha = 1$) at small separations and α decreases with increasing separation, with $\alpha \approx 0$ (random overlap) for separations larger than ~3 km (Figs. 4a, 4c, and 4e). The exponential fit suggested by HI00 with $Z_0 = 1.4$ km shows reasonable agreement with the data at SGP. The value of Z_0 is unchanged when using the 1997–2002 period used by MBT02 and close to their value for winter data (see Table A1, the appendix). For the TWP sites, Z_0 values of 1.5 and 1.3 km are found at Manus and Nauru, respectively, close to the SGP value. However, these values are much smaller than those found in MBT02, mainly because of differences both in the method used to detect precipitation and in the maximum altitude allowed in the radar profiles (see the details in the appendix). Contiguous cloud layers at Manus (Fig. 4c) show a decay of α with separation but α converges toward a value of 0.1 rather than zero. Nauru data show a decay of α as a function of separation for contiguous cloud layers, a tendency toward negative values, and considerable variability at large separations (Fig. 4e).

For noncontiguous layers, α for the three locations is more or less constant at all separations, with a negative value of slightly less than -0.1, suggesting random overlap in general and occasional minimum overlap (Figs. 4b, 4d, and 4f). This is in accordance with the results of HI00 and MBT02.

b. Impact of dynamics and thermodynamic state

To be useful for parameterization design, it is necessary for the overlap behavior we observe to be related to quantities predicted by a GCM. Using RUC-2 temperature, vertical velocity, geopotential height, and three-dimensional wind fields, we investigate how the distribution of α depends on the dynamics at SGP.

Figure 5a (top panels) shows the transition of α as a function of layer separation at SGP for four different 500-mb pressure level vertical velocity (ω) categories, and Fig. 5b shows the vertical distribution of cloud oc-

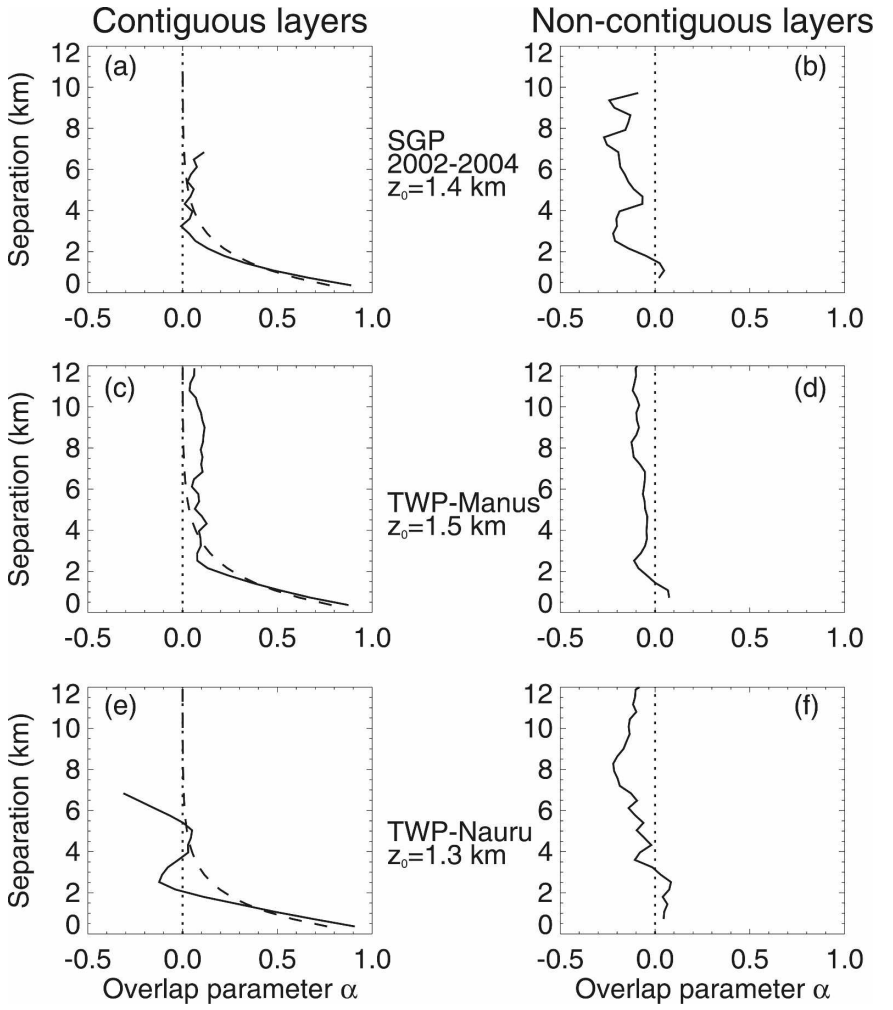

FIG. 4. Mean overlap parameter α as a function of layer separation for (left) contiguous and (right) noncontiguous cloud layers for (top) SGP-winter, (middle) TWP-Manus, and (bottom) TWP-Nauru. All curves stop at the cloud-layer separation for which the number of points is less than 250. The dashed line is the exponential fit to the contiguous cloud-layer data suggested by HI00 with the corresponding Z_0 value provided to the right of the graph.

currence at times when the overlap of the contiguous layers is calculated. The cloud profiles are similar for all ω but extend somewhat deeper on average when upward motion ($\omega < 0$) exists at 500 mb. The distance between cloud layers over which the overlap changes from maximum to random (Z_0) is similar and fairly small in descending ($\omega > 0$) regimes and mildly ascending regimes. In fact, α is marginally negative for separations >2.5 km. However, large negative values of ω tend to abruptly increase Z_0. Under these conditions, α actually never approaches zero. In other words, vigorous ascent tends to favor maximum overlap. The greatest ascent threshold is roughly indicative of vertical velocities that are typical of frontal regions in baroclinic storms (see Fig. 3 of Naud et al. 2006). Furthermore, the sense of ARSCL–merged moments systematic differences (Fig. A1b, the appendix), which we expect to exist primarily for strong upward ascent, would only amplify the dependence of α on ω.

We selected subsets of the SGP data for which ω at 500 mb is positive (i.e., downward) and compared mean α for the points below the 25th and above the 75th percentiles of the vertical shear of the horizontal wind (see Table 1). The wind shear is calculated between the two cloud layers used to calculate α. From Fig. 6a, we observe that wind shear slightly affects overlap for separations greater than 2 km, increasing the occurrence of minimum overlap, but the difference in α between weak and large wind shears is barely greater than 0.1 at ~3 km.

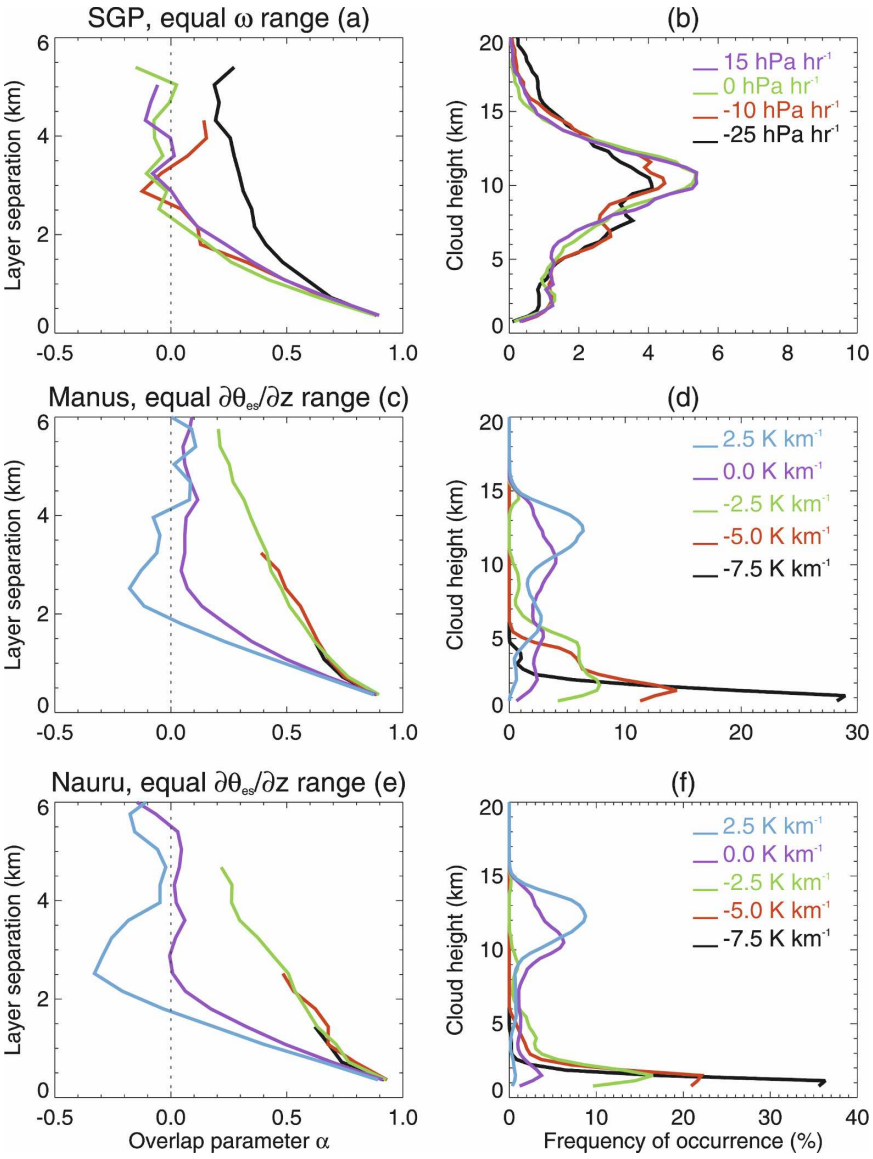

FIG. 5. Mean overlap parameter α as a function of separation: (a) at SGP for all winter months of 2002–2004 and for four subsets of increasing 500-mb ω such as $\omega < 15$ hPa h^{-1}, $-15 < \omega < -5$ hPa h^{-1}, $-5 < \omega < 5$ hPa h^{-1}, and $\omega > 5$ hPa h^{-1}; (c) at Manus for five subsets of increasing $\partial\theta_{es}/\partial z$; and (e) as in (c) but for Nauru. The TWP $\partial\theta_{es}/\partial z$ subsets are 2.5 K km^{-1} wide and centered on 2.5, 0, -2.5, -5, and -7.5 K km^{-1}; the range defined by -7.5 K km^{-1} also includes all of the points found below -8.75 K km^{-1}. All curves stop at the separation where the number of points <250 at SGP but the criterion was relaxed to 100 points at TWP. For each site, the right column shows the height distribution of all layers that were used to obtain the overlap parameter (no overcast cloud sublayers).

For the TWP sites, vertical velocities are poorly constrained by observations and determined largely by uncertain aspects of model moist physics in the 6-hourly NCEP–NCAR reanalysis. This may explain why α shows no dependence on 500-mb ω at these sites. Instead, we calculate the vertical gradient, between the two layers used to calculate α, of saturation equivalent potential temperature ($\partial\theta_{es}/\partial z$), which is diagnostic of the degree of conditional instability to moist convection:

$$\theta_{es} = \theta \exp\left(\frac{L_v \omega_s}{C_p T}\right), \tag{3}$$

with θ the potential temperature, L_v the latent heat of vaporization, ω_s the saturation mixing ratio, C_p the spe-

TABLE 1. Number of points per quartile and corresponding threshold for the wind shear subsets examined at SGP, Manus, and Nauru.

Location	Regime	No. of points per quartile	Shear threshold (m s^{-1}) km^{-1}
SGP	Subsidence: low shear	8059	<1.79
	Subsidence: large shear	8058	>4.79
Manus	Stable: low shear	16 023	<0.55
	Stable: large shear	16 021	>1.93
Nauru	Nauru low shear	7062	<0.58
	Nauru large shear	7062	>2.21

cific heat at constant pressure, and T the temperature. Figures 5c and 5e show the variation of α as a function of separation at Manus (middle panels) and Nauru (bottom panels) once the datasets are partitioned into five ranges of $\partial\theta_{es}/\partial z$, from convectively unstable to stable. For these curves we relaxed the threshold of a 250-point minimum at each separation to a 100-point minimum to allow for separations greater than 1 km to be represented in several categories. When the situation is unstable (i.e., $\partial\theta_{es}/\partial z < 0$ K km^{-1}) there is no dependence of α on the magnitude of $\partial\theta_{es}/\partial z$. Under these conditions the curves asymptotically converge at large separations to a value of $\alpha > 0$, indicating that maximum overlap occurs often over great depth. As $\partial\theta_{es}/\partial z$ becomes positive and increases toward greater stability, the overlap gradually becomes random for separations >2 km. There is a slight deviation of α toward negative values for the most stable situations, indicating that sometimes the overlap is minimum in the most stable conditions.

Figures 5d and 5e show the distributions of the altitudes of the cloudy layers that were used to evaluate α in each $\partial\theta_{es}/\partial z$ range at the TWP sites. The figures show that negative values of $\partial\theta_{es}/\partial z$ are associated with low-level cloud layers that are confined to the part of the troposphere where instability is greatest. Large positive $\partial\theta_{es}/\partial z$ is associated with clouds in the stable upper troposphere. In other words, the stability variations seen in Fig. 5 for the TWP sites represent mostly differences between the lower and upper troposphere rather than variations in time of the atmospheric state. It is therefore possible that the overlap dependence on $\partial\theta_{es}/\partial z$ reflects differences of some other kind between low-level and high-level clouds rather than an inherent effect of stability, but we did not find any evidence of such factors. We verified that calculating $\partial\theta_{es}/\partial z$ between two fixed levels in the lower troposphere (e.g., 600 and 1000 mb, the layer below the θ_{es} minimum) also reveals a tendency for the more unstable situations to favor maximum rather than random overlap at large

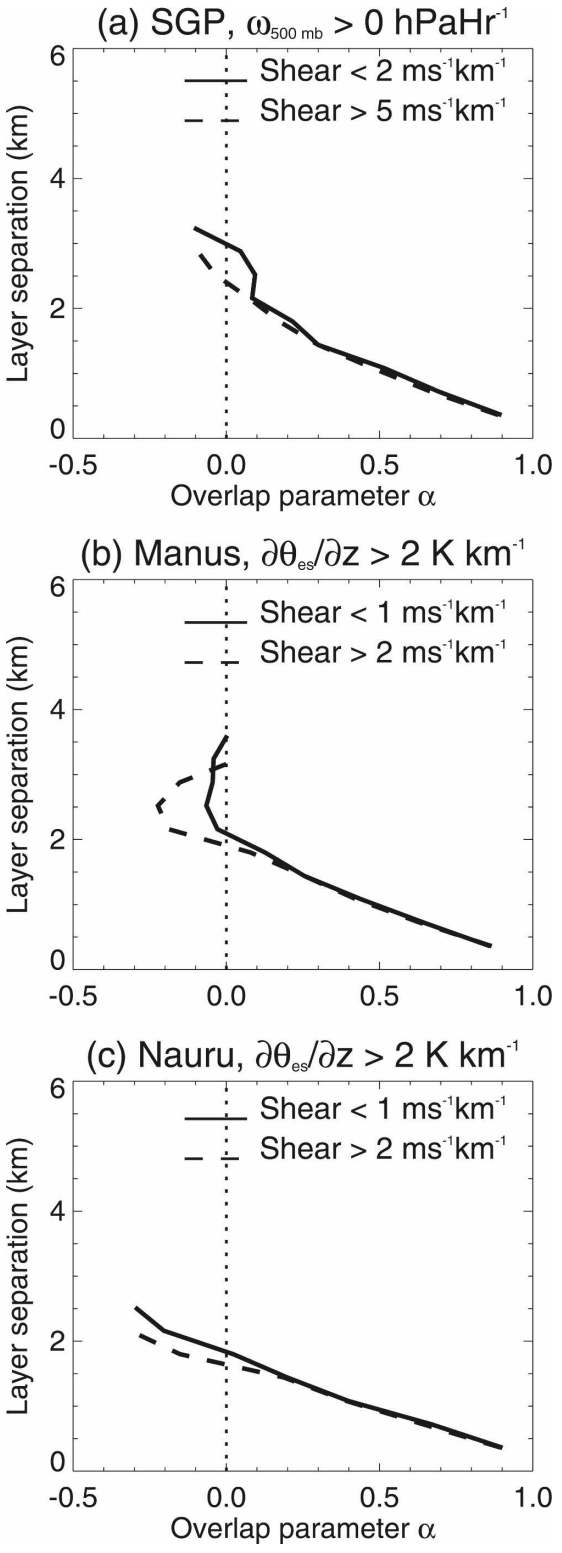

FIG. 6. Mean overlap parameter α as a function of separation for the two subsets derived from the 25th (solid) and 75th (dashed) distributions of the wind shear: (a) at SGP for all points in descending situations, (b) at Manus for $\partial\theta_{es}/\partial z > 1.7$ K km^{-1} (75th percentile of the $\partial\theta_{es}/\partial z$ distribution), and (c) at Nauru for $\partial\theta_{es}/\partial z > 2.1$ K km^{-1} (75th percentile of the $\partial\theta_{es}/\partial z$ distribution). All curves stop at the separation where the number of points <250.

separations. However, the range of $\partial\theta_{es}/\partial z$ temporal variation in the tropical lower troposphere is only about ± 2 K km^{-1}, too small for the difference in mean α to be greater than the uncertainty of 0.1.

In stable situations ($\partial\theta_{es}/\partial z > 1.7$ and 2.1 K km^{-1} at Manus and Nauru, respectively) the wind shear between the cloud layers used to calculate α has a similar effect on α as it does at the SGP (see Table 1 for the thresholds). At both sites (Figs. 6b and 6c) large wind shear favors minimum overlap at large separations more often than weak shear does, although at Nauru there is a minimum overlap tendency even without large wind shear.

We also examined the dependence of α on the dynamic and thermodynamic state for noncontiguous cloud layers at all three sites but fewer points exist and the change in mean α is smaller than the uncertainty defined earlier, preventing us from drawing any definite conclusions. If there is an impact of the dynamics or atmospheric state on the overlap between noncontiguous layers, it is apparently rather small.

c. *Sensitivity to spatial and temporal resolution*

HI00 found that Z_0 decreases with increasing spatial and temporal resolution. MBT02 also found a decrease in Z_0 with increasing temporal resolution at all sites but SGP while they find a decrease in Z_0 with decreasing spatial resolution. We found a decrease in Z_0 with increasing resolution at SGP for the winter months. We tested how different spatial and temporal resolutions affect the impact of the atmospheric state on overlap, using data from Nauru. We used 180- and 1080-m layers rather than 360-m layers for 1-h periods and found, as before, an increase in maximum overlap occurrence in unstable situations. Keeping the 360-m layers but changing the 1-h period to 20 min and 3 h, again we observe the same strong signal. What changes from one resolution to another is the number of points available per cloud layer separation, which in turn affects the thresholds on the vertical velocity and saturation equivalent potential temperature gradients. Wind shear effects on overlap were found to be marginal when there were enough points, even for 180-m/1-h resolution data that give the largest number of points.

4. Discussion and conclusions

Starting from the method of Hogan and Illingworth (2000), we have explored the relationship between cloud vertical overlap and dynamics using radar cloud masks from the SGP and TWP sites. We reproduced the HI00 results at a different midlatitude location in winter. Our results are also in accordance with those obtained by Mace and Benson-Troth (2002) for the cold season at SGP using a different radar cloud mask, but differences in the method used to eliminate precipitating periods and in the upper limit on cloud altitude cause disagreements between the two studies, in particular at the TWP sites.

For winter months at a midlatitude continental site, overlap at large separations is affected by strong midtropospheric vertical motion, while in the tropics it is related to convective instability. Random or minimum overlap occurs preferentially in regions of subsidence or convective stability, maximum overlap preferentially in strong ascent, or convectively unstable conditions. In situations of small or descending velocities in midlatitudes, we find that large wind shear favors minimum overlap and, similarly at TWP, in convectively stable situations. At all locations, no significant impact of the dynamics or atmospheric state was found for noncontiguous cloud layers. A similar impact of the dynamics or atmospheric state on cloud overlap was found at different temporal and spatial resolutions of the radar cloud mask.

The overlap parameter α does not asymptotically approach zero at large separations in dynamically active environments. Thus, there is no straightforward way to apply the exponential fits of HI00 directly to create an improved overlap parameterization that is sensitive to the atmospheric state.

We suggest instead that fairly straightforward modifications to the existing mixed maximum–random overlap parameterization currently used in many GCMs might capture most of the important variability. Overlap is an inherently statistical property of GCM cloud parameterizations; that is, it is not possible to calculate the instantaneous overlap in a GCM grid box accurately. Our results might be used to probabilistically switch the overlap of contiguous cloud layers from maximum to random, as was done in Räisänen et al.'s (2004) "cloud generator," but as a function of the large-scale vertical velocity or convective instability. For noncontiguous cloud layers, the existing assumption of random overlap appears to be generally valid, although the hint of a nonzero minimum overlap contribution in our results suggests that assuming minimum overlap a small fraction of the time, applied randomly, might help increase cloud cover, which is often underestimated by models (e.g., Weare 2004; GFDL Global Atmospheric Model Development Team 2004; Schmidt et al. 2006). A similar consideration applies to contiguous cloud layers in the presence of strong wind shear. The observed exponential dependence of α on separation for all conditions combined shown by HI00, MBT02, and in this

paper would then become a metric for parameterization evaluation rather than a parameterization itself. The benefit of a physics-based overlap approach would be its predictive potential for climate change, since such an approach would allow for the possibility of cloud overlap feedback. The development and testing of such a parameterization will be the object of future investigation.

In this study radar data from two locations in different climate regimes were used. To determine whether the relationships between dynamics and cloud overlap we describe here are generally applicable, a global dataset is needed. Using a spaceborne lidar, Wang and Dessler (2006) looked at a month's worth of cloud vertical profiles and found some discrepancies between the current assumption of random overlap between noncontiguous cloud layers and their measurements. However, lidars tend to be attenuated rapidly in optically thick cloud, which prevents one from observing situations with more than one cloud layer where the highest layer has an optical depth larger than 3 (e.g., anvils overlying low-level clouds). On the contrary, millimeter-wave radars can sample these situations, attenuation coming mainly from precipitation (large particles), which is less of a problem if clouds are observed from space. Spaceborne radars (e.g., CloudSat; Stephens et al. 2002) present the additional advantage of allowing a systematic and global analysis and, in addition, with their two-dimensional profiles of radar vertical distribution, will help to verify that the one-dimensional data collected at ground sites give an accurate picture.

Acknowledgments. This work was supported by an interagency agreement with the Atmospheric Radiation Measurement program of the U.S. Department of Energy. EEC was supported by the Office of Science (BER), U.S. Department of Energy, Grant DE-FG02-90ER61071. GGM and SB were also supported by the Office of Science (BER), U.S. Department of Energy, Grant DE-FG03-98ER62571. NCEP reanalysis data were provided by the NOAA/OAR/ESRL PSD, Boulder, Colorado, from their Web site (http://www.cdc.noaa.gov). The authors thank Robin Hogan and an anonymous reviewer for their very helpful remarks.

APPENDIX

Comparison between ARSCL and MBT02 Cloud Masks

In section 3a, Z_0 at the three sites differs from the MBT02 estimates obtained with the same radars. Three different reasons for this discrepancy were found and are discussed here: the cloud mask, the precipitation removal method, and the maximum altitude of clouds allowed in the profiles.

MBT02 did not use the ARSCL cloud mask but the "merged moments" mask described in Mace et al. (2006). The ARM radar observations are obtained from four different modes, which are sensitive to different altitudes and types of clouds and activated consecutively over about 40 s. The merged moments mask was obtained primarily from the general and cirrus modes and provides the data on the native 90-m and 40-s grid (Mace et al. 2006). ARSCL combines the four available modes (Clothiaux et al. 2000) and interpolates them onto a 10-s grid.

The net result is that ARSCL gives larger cloud fractions than does merged moments. For January 1999 at SGP, including precipitation periods, 38% of the cloudy layers were overcast with the ARSCL cloud mask versus 24% with merged moments. This caused day-to-day differences in Z_0 between the two masks but a minimum of 10 days showed a convergence of the difference within 1 km. For the entire month, cloud fractions have to be calculated over time periods of at least 1 h for a convergence within a few hundred meters or better. This is only slightly longer than a typical GCM physics time step and shorter than the time scale of most radiation–dynamics interactions. To evaluate the systematic uncertainty in α introduced by the cloud mask, data obtained at SGP for winter months from 1997 to 2000 were selected and the difference between the merged moments and the ARSCL mean α was plotted as a function of separation (Fig. A1), fixing the maximum altitude to 10.5 km in the ARSCL dataset and only keeping separations for which at least 250 points are available in both sets. Overall, Fig. A1b reveals that when precipitation periods are kept in ARSCL, the agreement between the two cloud masks is always within the 0.1-α requirement (see section 2c) while when they are removed, the differences are more negative though still near the 0.1-α requirement.

The effects on Z_0 of the method chosen to remove periods of precipitation and of leaving clouds above 10.5 km in the radar profiles are examined using the ARSCL dataset for the three locations and the time periods used here (see Table A1). MBT02 estimates of Z_0 are also included for comparison (SGP 1997–2000 winter data had to be processed specifically).

Precipitation artificially increases overlap in radar data, so Z_0 is lower at all three sites when precipitating periods are removed in the ARSCL dataset (Table A1, column c). MBT02 and ARSCL Z_0 agree closely only when the precipitating periods are kept in the ARSCL dataset at all three sites (Table A1, column a) because

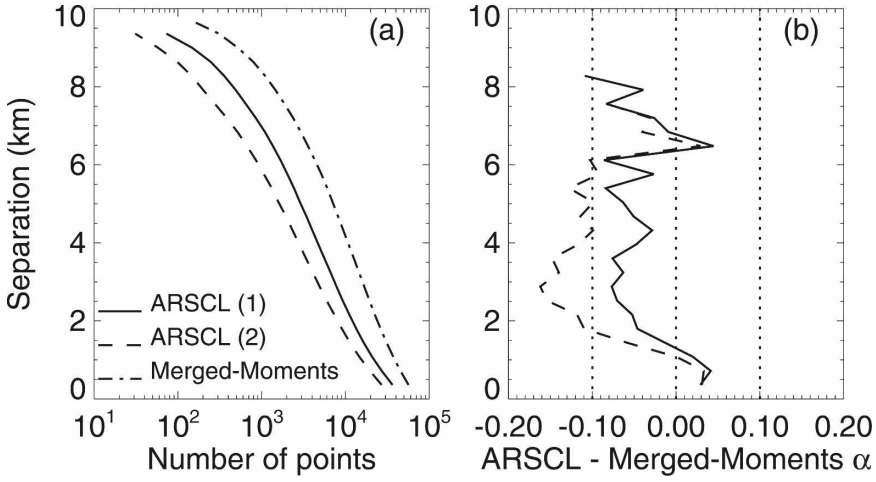

FIG. A1. Comparison between ARSCL and merged moments for SGP-winter, 1997–2000. (a) The number of points per layer separation for all ARSCL periods (1; solid), ARSCL without precipitation periods (2; dashed), and merged moments (dotted–dashed) are illustrated. (b) The differences in mean α between ARSCL-1 and merged moments (solid) and ARSCL-2 and merged moments (dashed) are illustrated as a function of layer separation.

the ARSCL identification of the precipitating periods is more restrictive than the method used in MBT02 (their method is based on information contained in the radar returns and temperature profiles). Figure A2a shows, for Manus where the impact of precipitation on Z_0 is largest, the raw radar reflectivity time series as a function of altitude, the coincident micropulse lidar derived cloud-base height (from the ARSCL files), and the time steps when the rain gauge detected precipitation for 15 Dec 1999. Figure A2b shows the same reflectivities once the ARSCL cloud mask was applied and the precipitation periods removed, while Fig. A2c shows the reflectivities after the merged moments cloud and precipitation mask was applied. During the period of intense precipitation (0100–0230 UTC), no overlap parameter is derived with ARSCL, while as Fig. A2c reveals, some precipitation periods were kept in the MBT02 dataset. The latter method can keep some of the precipitating clouds and clouds that may be above and not connected to precipitating clouds. The larger Z_0 found in MBT02 when compared to Z_0 obtained with ARSCL in dry periods can thus also be caused by the overlap properties of precipitating clouds and those clouds that may occur aloft. Figure A2 also reveals the problem of radar attenuation caused by large and numerous precipitating particles: cloud-top heights decrease with the onset of precipitation and sharply go up again as it finishes. Attenuation creates artificial breaks in clouds, giving a maximum cloud overlap. This problem occurs in periods when the precipitation rate exceeds 5 mm h^{-1} and the liquid water column exceeds about 1 cm. This is more of a problem at the tropical

TABLE A1. Estimates of Z_0 (km) for the entire periods used in MBT02 at Manus, Nauru, and SGP-winter. The Manus and Nauru MBT02 Z_0 values come from Table 3 of MBT02. The SGP-winter estimate was calculated specifically for this study using data from November–March 1997–2000. Values from ARSCL are given for (a) precipitating periods that are kept and the maximum altitude $Z_{max} = 10.5$ km, as in MBT02; (b) precipitating periods that are kept but $Z_{max} > 10.5$ km; (c) precipitating periods that are removed and $Z_{max} = 10.5$ km; and (d) precipitating periods that are removed and $Z_{max} > 10.5$ km. For (b) and (d), the maximum altitude available is 15 km at SGP and 20 km at TWP.

		ARSCL Z_0 (km)			
		(a)	(b)	(c)	(d)
Location	MBT02 Z_0 (km)	With precipitating periods $Z_{max} = 10.5$ km	With precipitating periods $Z_{max} > 10.5$ km	No precipitating periods $Z_{max} = 10.5$ km	No precipitating periods $Z_{max} > 10.5$ km
Manus	4.0	3.8	2.4	2.6	1.5
Nauru	4.6	4.2	1.8	3.2	1.3
SGP-winter (Nov–Mar)	1.9	1.7	1.5	1.6	1.4

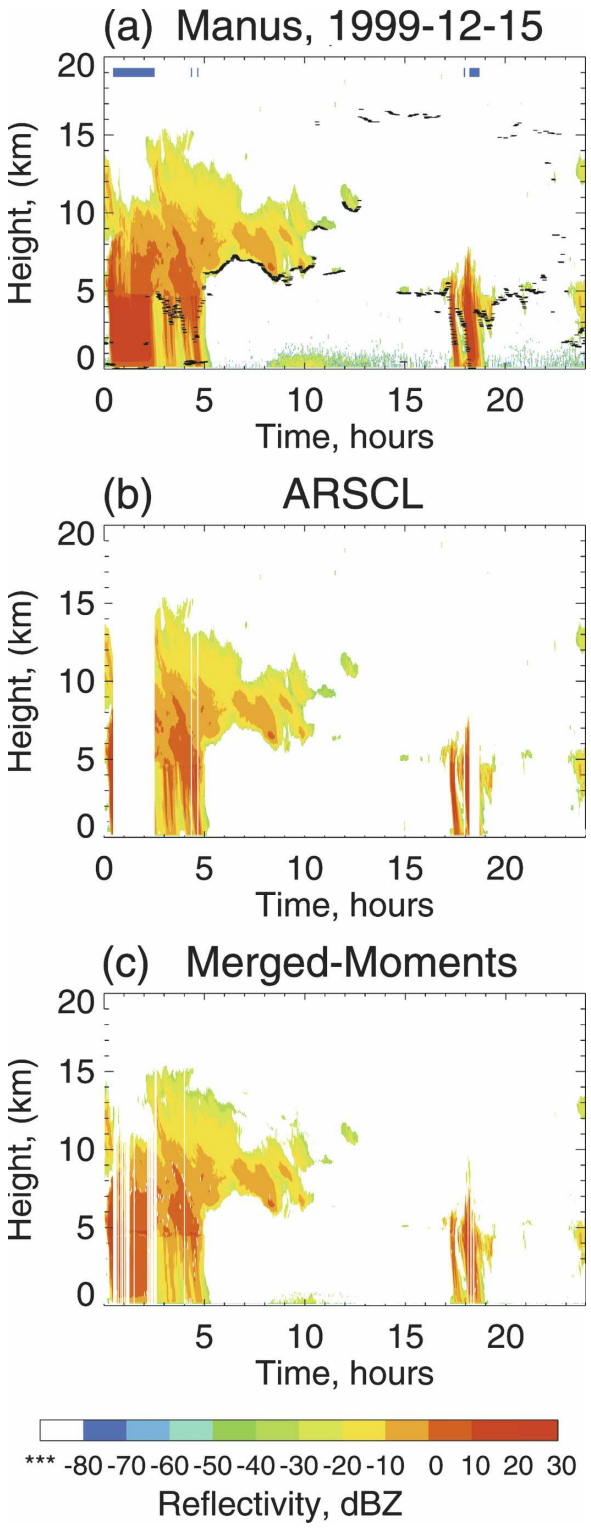

FIG. A2. For Manus, 15 Dec 1999: (a) the raw ARSCL radar reflectivity profiles, lidar cloud-base best estimate (black dashes), and, at the 19-km level, the time steps when precipitation was detected by the rain gauge (blue vertical bars) as a function of time; (b) the ARSCL best-estimate radar reflectivity profiles with clear and clutter pixels and precipitating periods masked; and (c) the merged moments reflectivities with clear and clutter pixels and precipitating periods masked.

sites than at SGP in winter. However, in dry periods, there is no correlation between changes in liquid water path and in cloud-top height. So, in this paper, to avoid contamination by both precipitation and attenuation, the optical rain gauge and condensation sensor strip indicators are used to completely exclude hourly periods that contain precipitation.

Finally, when the ARSCL data are extended from 10.5 km to the highest possible levels of 15 and 20 km at SGP and TWP, respectively, Z_0 significantly decreases (Table A1, column b). Therefore, clouds that are normally present above 10.5 km at all three sites, but especially in the tropics, tend to exhibit random overlap. Together, the precipitation removal technique and the choice of cloud maximum altitude explain the much smaller Z_0's in section 4 of this paper than in MBT02 (Table A1, column d).

REFERENCES

Ackerman, T. P., and G. M. Stokes, 2003: The Atmospheric Radiation Measurement program. *Phys. Today,* **56,** 38–44.

Benjamin, S. G., J. M. Brown, K. J. Brundage, B. E. Schwartz, T. G. Smirnova, and T. L. Smith, 1998: The operational RUC-2. Preprints, *16th Conf. on Weather Analysis and Forecasting,* Phoenix, AZ, Amer. Meteor. Soc., 249–252.

Chen, T., Y. Zhang, and W. B. Rossow, 2000: Sensitivity of atmospheric radiative heating rate profiles to variations of cloud layer overlap. *J. Climate,* **13,** 2941–2959.

Clothiaux, E. E., T. P. Ackermann, G. C. Mace, K. P. Moran, R. T. Marchand, M. A. Miller, and B. E. Martner, 2000: Objective determination of cloud heights and radar reflectivities using a combination of active remote sensors at the ARM CART sites. *J. Appl. Meteor.,* **39,** 645–665.

Geleyn, J. F., and A. Hollingsworth, 1979: An economical analytical method for the computation of the interaction between scattering and line absorption of radiation. *Contrib. Atmos. Phys.,* **52,** 1–16.

GFDL Global Atmospheric Model Development Team, 2004: The new GFDL global atmosphere and land model AM2–LM2: Evaluation with prescribed SST simulations. *J. Climate,* **17,** 4641–4673.

Hogan, R. J., and A. J. Illingworth, 2000: Deriving cloud overlap statistics from radar. *Quart. J. Roy. Meteor. Soc.,* **126,** 2903–2909.

Kalnay, E., and Coauthors, 1996: The NCEP/NCAR 40-Year Reanalysis Project. *Bull. Amer. Meteor. Soc.,* **77,** 437–471.

Kistler, R., and Coauthors, 2001: The NCEP–NCAR 50-Year Reanalysis: Monthly means CD-ROM and documentation. *Bull. Amer. Meteor. Soc.,* **82,** 247–267.

Long, C. N., and T. P. Ackerman, 2000: Identification of clear skies from broadband pyranometer measurements and calculation of downwelling shortwave cloud effects. *J. Geophys. Res.,* **105,** 15 609–15 626.

——, ——, J. J. DeLuisi, and J. Augustine, 1999: Estimation of fractional sky cover from broadband SW radiometer measurements. Preprints, *10th Conf. on Atmospheric Radiation,* Madison, WI, Amer. Meteor. Soc., 383–386.

Mace, G. G., and S. Benson-Troth, 2002: Cloud-layer overlap

characteristics derived from long-term cloud radar data. *J. Climate,* **15,** 2505–2515.

——, and Coauthors, 2006: Cloud radiative forcing at the Atmospheric Radiation Measurement program Climate Research Facility: 1. Technique, validation and comparison to satellite-derived diagnostic quantities. *J. Geophys. Res.,* **111,** D11S90, doi:10.1029/2005JD005921.

Moran, K. P., B. E. Martner, M. J. Post, R. A. Kropli, D. C. Welsh, and K. B. Widener, 1998: An unattended cloud-profiling radar for use in climate research. *Bull. Amer. Meteor. Soc.,* **79,** 443–455.

Morcrette, J.-J., and C. Jakob, 2000: The response of the ECMWF model to changes in the cloud overlap assumption. *Mon. Wea. Rev.,* **128,** 1707–1732.

Naud, C. M., A. Del Genio, and M. Bauer, 2006: Observational constraints on cloud thermodynamic phase in midlatitude storms. *J. Climate,* **19,** 5273–5288.

Pincus R., C. Hannay, S. A. Klein, K.-M. Xu and R. Hemler, 2005: Overlap assumptions for assumed probability distribution function cloud schemes in large-scale models. *J. Geophys. Res.,* **110,** D15S09, doi:10.1029/2004JD005100.

Räisänen, P., H. W. Barker, M. F. Khairoutdinov, J. Li, and D. A. Randall, 2004: Stochastic generation of subgrid-scale cloudy columns for large-scale models. *Quart. J. Roy. Meteor. Soc.,* **130,** 2047–2067.

Schmidt, G. A., and Coauthors, 2006: Present-day atmospheric simulations using GISS ModelE: Comparison to in situ, satellite, and reanalysis data. *J. Climate,* **19,** 153–192.

Stephens, G. L., and Coauthors, 2002: The CloudSat mission and the A-Train: A new dimension of space-based observations of clouds and precipitation. *Bull. Amer. Meteor. Soc.,* **83,** 1771–1790.

Wang, L., and A. E. Dessler, 2006: Instantaneous cloud overlap statistics in the tropical area revealed by ICESat/GLAS data. *Geophys. Res. Lett.,* **33,** L15804, doi:10.1029/2005GL024350.

Weare, B. C., 2004: A comparison of AMIP II model cloud layer properties with ISCCP D2 estimates. *Climate Dyn.,* **22,** 281–292.